




Linear response theory of open systems with exceptional points

A. Hashemi ^{1,2✉}, K. Busch^{3,4}, D. N. Christodoulides ⁵, S. K. Ozdemir ⁶ & R. El-Ganainy^{1,2✉}

Understanding the linear response of any system is the first step towards analyzing its linear and nonlinear dynamics, stability properties, as well as its behavior in the presence of noise. In non-Hermitian Hamiltonian systems, calculating the linear response is complicated due to the non-orthogonality of their eigenmodes, and the presence of exceptional points (EPs). Here, we derive a closed form series expansion of the resolvent associated with an arbitrary non-Hermitian system in terms of the ordinary and generalized eigenfunctions of the underlying Hamiltonian. This in turn reveals an interesting and previously overlooked feature of non-Hermitian systems, namely that their lineshape scaling is dictated by how the input (excitation) and output (collection) profiles are chosen. In particular, we demonstrate that a configuration with an EP of order M can exhibit a Lorentzian response or a super-Lorentzian response of order M_s with $M_s = 2, 3, \dots, M$, depending on the choice of input and output channels.

¹Department of Physics, Michigan Technological University, Houghton, MI 49931, USA. ²Henes Center for Quantum Phenomena, Michigan Technological University, Houghton, MI 49931, USA. ³Humboldt-Universität zu Berlin, Institut für Physik, AG Theoretische Optik & Photonik, D-12489 Berlin, Germany. ⁴Max-Born-Institut, Max-Born-Straße 2A, 12489 Berlin, Germany. ⁵CREOL/College of Optics and Photonics, University of Central Florida, Orlando, FL 32816, USA. ⁶Department of Engineering Science and Mechanics, and Materials Research Institute, The Pennsylvania State University, University Park, PA 16802, USA. ✉email: hashemis@mtu.edu; ganainy@mtu.edu

Resonance is a universal physical phenomenon that takes place in a large variety of systems across a wide range of spatial and time scales. In optics, the rapid progress in modeling and fabrication has enabled the realization of several photonic resonator structures that can trap light for very long times (high-quality factors)¹ or confine it in smaller domains compared with the free-space wavelength (nano-scale mode volumes)². These devices have become indispensable components in almost every field of optical science and engineering including but not limited to lasers, nonlinear optics, optical communication, quantum optics, and biophotonics. While the notion of a completely closed resonator is sometimes used as an idealization to simplify the analysis and to gain intuition, it is neither realistic nor desirable. Quite the opposite, it is necessary to have open channels between the interior of the resonator and its surrounding in order to facilitate the input/output coupling of light. Thus, even in the absence of material loss, optical resonators are fundamentally non-Hermitian—a fact that is often overlooked despite some early works that considered non-Hermitian effects in optical systems^{3,4}. These studies demonstrated how non-Hermitian effects in lasers leave their fingerprint on emission linewidth. Those early works, however, focused on situations where the system does not exhibit spectral singularities known as exceptional points (EPs) since this scenario was not relevant to the experimental setups under study at that time.

In recent years, the interest in non-Hermitian optical structures has acquired a new dimension following a number of theoretical studies of parity-time (PT) symmetry in optics^{5–7} and its first experimental demonstrations^{8,9}. This in turn has initiated intense theoretical^{10–39}, and experimental^{40–58} investigations of non-Hermitian effects in photonic platforms. In contrast to earlier studies, the notion of EPs is at the heart of these recent works. This in turn has initiated feverish efforts seeking to explore the exotic features of wave dynamics in waveguide and resonator geometries that exhibit EPs. For recent reviews, see refs. ^{59–64}. Despite these intense activities on the one hand, and the fact that the mathematics of non-self-adjoint operators is well developed on the other, some of the basic features of complex photonic structures that are pertinent to their non-Hermitian nature are either underestimated or misunderstood. Particularly, on one side of the spectrum, the prevailing traditional point of view treats openness only as a source of energy loss or gain, and hence relies completely on Hermitian intuition to analyze the system. On the other side, some works that deal with non-Hermitian systems exhibiting EPs tend to assume that the linear response associated with a defective Hamiltonian (i.e., a Hamiltonian whose spectrum has one or more EPs) can be studied only within the context of perturbation theory which is conceptually misleading even when the final results are mathematically correct.

Beyond this fundamental issue, the perturbative analysis can be cumbersome and complex for non-Hermitian arrangements with large number of resonant elements, particularly when the spectrum contains several EPs, some of which exhibit higher orders. This situation becomes relevant for example when studying non-Hermitian topological arrangements^{65–68}, non-Hermitian disordered media^{69–71}, as well as non-Hermitian spin systems where the number of EPs scale exponentially with the system's size⁷². In addition, the recent discovery of non-Hermitian systems that exhibit exceptional surfaces (ESs) rather than EPs introduces another hurdle for applying perturbation expansions. Figure 1b illustrates this point. The perturbation analysis used to study a defective Hamiltonian \hat{H}_{EP} typically starts by introducing a perturbation Hamiltonian $\epsilon\hat{H}_{\text{pt}}$ that removes the non-Hermitian degeneracy. The resolvent of the resultant non-defective Hamiltonian $\hat{\mathcal{H}}_{\text{tot}} \equiv \hat{H}_{\text{EP}} + \epsilon\hat{H}_{\text{pt}}$, defined as $G(\omega; \epsilon) \equiv (\omega\hat{I} - \hat{\mathcal{H}}_{\text{tot}})^{-1}$

where ω is the frequency and \hat{I} is the unit operator/matrix, can be then obtained using the left and right eigenstates. The resolvent of the defective Hamiltonian is obtained by evaluating $G_{\text{EP}}(\omega) = \lim_{\epsilon \rightarrow 0} G(\omega; \epsilon)$. Thus, in systems exhibiting exceptional surfaces, one first has to identify the hypersurface of all EPs and carefully identify perturbation Hamiltonians that force the system out of this hypersurface, otherwise the perturbation analysis will fail since $\hat{\mathcal{H}}_{\text{tot}}$ will be also defective (see Fig. 1b). This task is highly non-trivial since, for systems with large degrees of freedom, the exceptional surface is embedded in a space of high dimensionality. Importantly, taking the above limit involves cancellations of several infinite terms. As a result, any finitely small approximation in applying the perturbation analysis can lead to inconsistent results.

In addition to the above mathematical difficulties in using perturbative expansions to analyze defective Hamiltonians, the outcome of this analysis does not provide much insight into the role of non-Hermiticity in shaping the linear response of the system, specially when the latter exhibits many degrees of freedom and several input and output channels. In order to illustrate some of the subtleties arising in such systems in an intuitive way, and in doing so motivates our work, we consider the example shown in Fig. 2. It consists of three microring resonators that are coupled sequentially via horizontal waveguides. An additional vertical waveguide provides access to selectively excite the second resonator. We neglect the cross talk between the horizontal and vertical waveguides since it can be minimized using various design strategies^{73–76}. A similar system was considered in²⁹ and shown to exhibit a third-order EP in the subspace spanned by the clockwise (CW) and counterclockwise (CCW) modes of the resonators $R_{1,2,3}$. When the input/output channels are selected as shown in Fig. 2a, light will cross only cavity R_3 and hence the response features a Lorentzian function. On the other hand, for the channels depicted in Fig. 2b, input light will interact with both cavities $R_{2,3}$ in a series fashion before it exists. One thus expects a super-Lorentzian response of order two. Finally, for the input/output choice shown in Fig. 2c, light will traverse all three cavities in series which results in a super-Lorentzian response of order three (see Supplementary Note 1 for detailed analysis of this example). This rather intuitive example reveals that a system with EP of order three can exhibit very different response lineshapes depending on the choice of the input/output channel configuration—a feature that to the best of our knowledge has not been identified in non-Hermitian systems. Needless to say that in more complex structures, identifying the response corresponding to a given input/output channel configuration is not a trivial task.

The lesson learned from the above simple example is of extreme importance since many of the exotic and useful features of non-Hermitian systems with EPs arise due to the modified spectral lineshape. For instance, the recent work on EP-based optical amplifiers shows that the gain-bandwidth product of a resonant optical amplifier can be enhanced by operating at an EP, provided that the response lineshape features a super-Lorentzian response, with better results obtained for higher-order super-Lorentzians²⁹. In other settings, super-Lorentzian response could lead to narrower lineshapes, and eventually resulting in a stronger light-matter coupling, which can be utilized to enhance spontaneous emission^{20,31,77} and energy harvesting⁷⁸ among other potential applications. At the fundamental level, probing the quantum noise in non-Hermitian systems requires a proper characterization of the lineshape response at various output ports due to vacuum fluctuations-induced noise at the input channels, including loss and gain ones⁷⁹. Thus, in light of the above observation, it will be useful to develop a systematic, generic approach that establishes a universal relation between the response function and the input/output channel configuration.

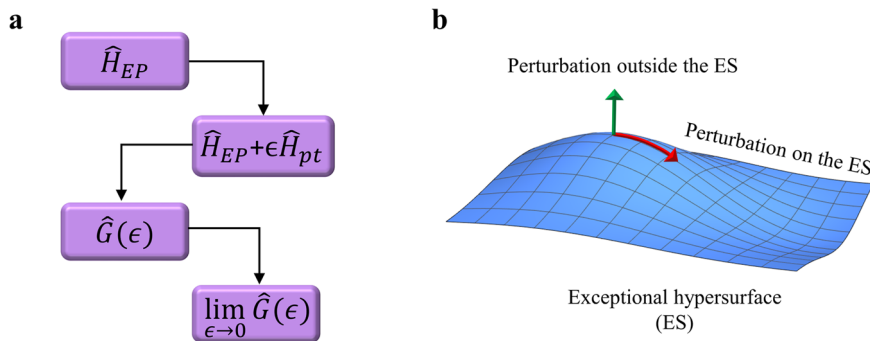


Fig. 1 Perturbation analysis of defective Hamiltonians (\hat{H}_{EP}) and its subtleties at exceptional surfaces. **a** Two crucial steps are involved: (1) finding a perturbation (\hat{H}_{pt}) that removes the degeneracy, and (2) obtaining the limit when the perturbation vanishes. $\hat{G}(\epsilon)$ is the Green operator. The first step can be straightforward in simple systems. **b** In systems that exhibit exceptional hypersurfaces in the parameter space^{23, 104, 125-127}, finding such a perturbation can be a very complex task since any perturbation that shifts the system along the surface will fail. In addition, taking the limit when $\epsilon \rightarrow 0$ involves the cancellation of several singular terms with opposite signs. For complex geometries with a large number of degrees of freedom, this can be a daunting task. In general, it is not possible a priori to confirm if this approach gives exact answer or approximate response function.

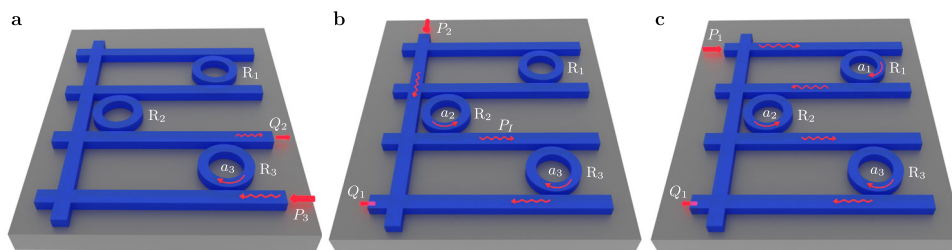


Fig. 2 Subtleties of linear response of non-Hermitian systems having EPs: an illustrative example. **a** An excitation (P_3) and collection (Q_2) scheme that leads to linear responses featuring Lorentzian lineshape. **b, c** Excitation ($P_{2,1}$) and collection (Q_1) schemes featuring super-Lorentzian responses of order two and three, respectively. Intuitively the order of the super-Lorentzian response depends on how many cavities the wave has traversed between the input and output ports. $a_{1,2,3}$ are cavity modes for ring resonators $R_{1,2,3}$, respectively.

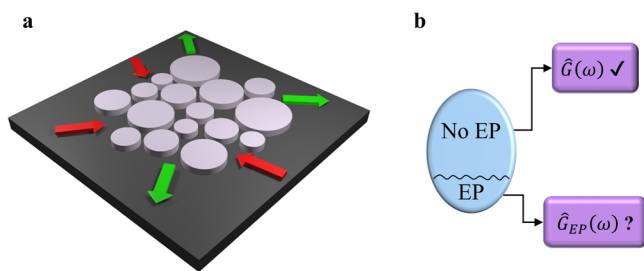


Fig. 3 Non-Hermitian resonant systems and their responses. **a** A schematic of a resonant open system, where non-Hermiticity arises due to coupling to external channels and the presence of optical loss or gain. As summarized in **(b)**, the linear response of this system, as described by its resolvent operator $\hat{G}(\omega)$ can be readily obtained in terms of the right/left eigenvectors of the associated non-Hermitian Hamiltonian when the spectrum of the latter does not contain any EPs. On the contrary, to date, a general expression for $\hat{G}_{EP}(\omega)$ in the presence of EPs has not been yet developed.

In this work, we bridge this gap and present a clear and general analysis of the linear response of any non-Hermitian resonant system. Figure 3a presents a schematic of one such a generic system, which consists of large number of coupled non-Hermitian resonators subject to an arbitrary specific choice of input/output channels. It is important to reiterate here that we focus on situations where the eigenvalue spectrum of the system exhibits EPs. While this situation represents a subset of the more general non-Hermitian family of Hamiltonians (see Fig. 3b), it is

by now understood that most of the novel behaviors of non-Hermitian systems arise when the system is at or near these EP singularities. In addition, in the absence of EPs, the system’s response can be easily obtained in terms of the left and right eigenvectors of the Hamiltonian. However, when EPs are present, the dimensionality of the eigenspace collapses and the analysis becomes complicated, thus prompting several authors to use perturbation methods as we described earlier. The main results of this work can be summarized as follows: (1) The linear response of resonator geometries that exhibit EPs can be obtained exactly without the need for perturbative expansions; (2) The Green’s function expansion can be used to tailor the response of the system by carefully selecting the input/output channels; (3) The excitation channels can be classified based on their interference properties; (4) The most efficient drive of the signal does not necessarily correspond to mode matching between the input signal and resonant modes. Importantly, we emphasize that even though we focus here on optical setups, due to the well-established mathematical analogy between this latter and other physical systems our results will be useful in analyzing and understanding other non-Hermitian platforms such as electronic^{80–84}, acoustic^{85–89}, mechanical^{90–92}, and thermal⁷⁸ systems.

Results

High-Q resonators can be strongly non-Hermitian. Before we proceed to the main topic of this work, it is instructive to first emphasize an important point that is sometimes overlooked in the literature, namely that non-Hermitian effects can be significant even in optical resonators with high-quality (Q) factors

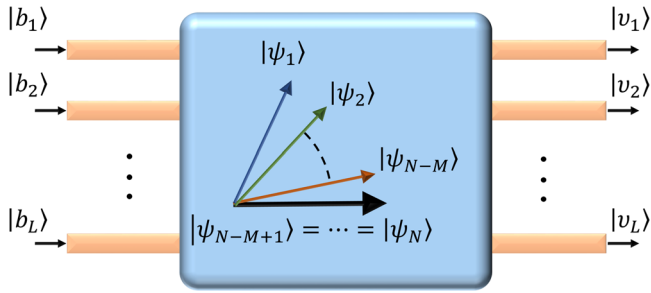


Fig. 4 A schematic of an open resonant structure with an EP and multiple input/output channels. As indicated by the structure of the eigenvectors $\{|\psi_n\rangle\}$, the spectrum of this resonant system is assumed to be of dimension N and having an EP of order M that arises due to gain/absorption or coupling to L input/output ports. $|b_i\rangle$ is the input signal from i th input port, and $|v_i\rangle$ is the output signal from i th output port.

(see, for instance, refs. 41,93). In general, the degree of non-Hermiticity can be assessed only by comparing the spatial scale of any non-Hermitian perturbation and its strength to the wavelengths of the resonant modes and their spectral separation, respectively. More specifically, if the non-Hermitian perturbation is spatially inhomogeneous and varies at a length scale comparable or smaller than the resonant wavelength, it can result in a measurable discrepancy between the lifetimes associated with different modes. In addition, the perturbation can also introduce hybridization between the bare modes. If such a modal mixing is induced by a coupling strength that is comparable to the frequency difference between the otherwise unperturbed modes, it could bring the system close to an EP. In that case, two or more of the eigenvectors of the system become very close (almost parallel). Obviously, in such a case, non-Hermitian effects beyond linewidth broadening cannot be neglected. A simple example that illustrates this point is the archetypal dimer configuration composed of two resonators having identical resonant frequency ω_o and two different loss factors $\gamma_{1,2}$. This system is described by a 2×2 Hamiltonian H with $H_{11,22} = \omega_o - i\gamma_{1,2}$ and $H_{12} = H_{21} = \kappa$ (we assume real coupling). If $\kappa = \Delta\gamma/2$ with $\Delta\gamma = (\gamma_2 - \gamma_1)$, the dimer will exhibit an EP. The quality factor associated with this degenerate mode is $Q = \frac{\omega_o}{2\bar{\gamma}}$, where $\bar{\gamma} = (\gamma_1 + \gamma_2)/2$. The above formulas do not impose any restrictions on Q , which can be engineered to be very large. Yet the system is highly non-Hermitian. The key observation here is that the perturbation $\Delta\gamma$, which introduces additional loss, is spatially inhomogeneous (affects only one site) and is comparable to the energy splitting of the unperturbed system 2κ . Examining the limit $\Delta\gamma = 0$ reveals that the eigenstates are orthogonal and the system does not exhibit any drastic non-Hermitian effect even if Q is designed to have a very low value. Thus, the important message here is that the degree of openness alone is insufficient to quantify if the system is highly non-Hermitian or not. This in turn highlights the need to exercise extreme caution when dealing with non-Hermitian systems.

Model and preparatory comments. Within the context of temporal coupled-mode formalism⁹⁴, a complex resonant photonic structure (see Fig. 4) under linear conditions can be modeled by the following set of equations:

$$i \frac{d|a(t)\rangle}{dt} = \hat{\mathcal{H}}|a(t)\rangle + i\hat{\Gamma}|b(t)\rangle \quad (1)$$

$$|v(t)\rangle = \hat{Y}|b(t)\rangle - \hat{\Gamma}^T|a(t)\rangle,$$

where the kets $|a(t)\rangle = [a_1(t), a_2(t), \dots, a_N(t)]^T$, $|b(t)\rangle = [b_1(t), b_2(t), \dots, b_L(t)]^T$, and $|v(t)\rangle = [v_1(t), v_2(t), \dots, v_L(t)]^T$ represent the modal amplitudes of the resonant modes

and the input and the output channels, respectively. The $N \times N$ time-independent non-Hermitian matrix Hamiltonian $\hat{\mathcal{H}}$ characterizes coupling between the different resonant states, whereas the $L \times L$ matrix \hat{Y} quantifies the direct scattering between incoming and outgoing channels. Finally, the $N \times L$ matrix $\hat{\Gamma}$ describes the coupling between the N resonant modes and the L input/output channels. To simplify the notations, we also define $|f(t)\rangle \equiv i\hat{\Gamma}|b(t)\rangle$. The general solution to Eq. (1) that takes into account the transient response can be obtained by using Laplace transform. Here, however, we are interested in the steady-state response $|A(\omega)\rangle$, which can be expressed in terms of the frequency domain resolvent (sometimes also called Green's operator or function) $\hat{G}(\omega) \equiv (\omega\hat{I} - \hat{\mathcal{H}})^{-1}$ (i.e., \hat{I} is the unit operator) as:

$$|A(\omega)\rangle = \hat{G}(\omega)|F(\omega)\rangle, \quad (2)$$

where $|A(\omega)\rangle \equiv \mathcal{FT}(|a(t)\rangle)$ and $|F(\omega)\rangle \equiv \mathcal{FT}(|f(t)\rangle)$ with $\mathcal{FT}(\cdot)$ denoting the Fourier transform. Before we proceed, we emphasize that the existence of a finite response (i.e., non-diverging resolvent) is not always guaranteed as we will discuss in more detail later.

To keep the discussion focused, we will only consider an excitation vector $|f(t)\rangle$ with separable time dependence and spatial profile, i.e., $|f(t)\rangle = s(t)|u\rangle$ where $s(t)$ is a scalar function of time and $|u\rangle = [u_1, u_2, \dots, u_N]^T$ is a time-independent excitation profile vector. In the frequency domain, the excitation vector thus takes the form $|F(\omega)\rangle = S(\omega)|u\rangle$. The eigenvectors of the non-Hermitian $\hat{\mathcal{H}}$ defined by the set $\{|\psi_n^r\rangle : \hat{\mathcal{H}}|\psi_n^r\rangle = \Omega_n|\psi_n^r\rangle, \langle\psi_n^r|\psi_n^r\rangle = 1\}$ have the following two important properties: (1) The eigenvalues Ω_n are in general complex; and (2) The eigenvectors $|\psi_n^r\rangle$ do not need to be orthogonal. In the absence of EPs, the eigenvectors form a complete basis, hence we can represent any input profile using the expansion $|u\rangle = \sum_{n=1}^N c_n|\psi_n^r\rangle$, which in turn reduces Eq. (2) to:

$$\frac{|A(\omega)\rangle}{S(\omega)} = \sum_{n=1}^N \frac{c_n}{\omega - \Omega_n} |\psi_n^r\rangle. \quad (3)$$

Note, however, that the expansion coefficients c_n cannot be calculated using the usual projection $\langle\psi_n^r|u\rangle$. Instead, one has to employ the left eigenvectors of $\hat{\mathcal{H}}$, defined by $\{\langle\psi_n^l| : \langle\psi_n^l|\hat{\mathcal{H}} = \Omega_n\langle\psi_n^l|, \langle\psi_n^l|\psi_n^r\rangle = \delta_{n,m}\}$, to obtain $c_n = \langle\psi_n^l|u\rangle$ (see Supplementary Note 2 for more details). This is known as bi-orthogonal projection. The alerted reader will notice that we dropped the normalization condition $\langle\psi_n^l|\psi_n^r\rangle = 1$ from the definition of $\langle\psi_n^l|$. In fact, it can be shown that, for non-normal matrices, the conditions $\langle\psi_m^l|\psi_n^r\rangle = \delta_{n,m}$, $\langle\psi_n^l|\psi_n^r\rangle = 1$ cannot be satisfied simultaneously⁴ (see Supplementary Note 3).

By using $c_n|\psi_n^r\rangle = \langle\psi_n^l|u\rangle|\psi_n^r\rangle = |\psi_n^r\rangle\langle\psi_n^l|u\rangle$, and by assuming that the non-orthogonal basis are complete, we can express the resolvent as^{20,91}:

$$\hat{G}(\omega) = \sum_{n=1}^N \frac{|\psi_n^r\rangle\langle\psi_n^l|}{\omega - \Omega_n}. \quad (4)$$

Even without considering the effect of EPs, the above results already lead to counterintuitive results. For instance, energy transfer from an excitation signal to a particular eigenmode of the system can still take place even when their Hermitian overlap vanishes. In order to illustrate this, consider an input signal $|u\rangle = \frac{|\psi_m^r\rangle}{\langle\psi_m^r|\psi_m^r\rangle} - |\psi_n^r\rangle$ with $\langle\psi_m^r|\psi_n^r\rangle \neq 0$ (due to non-Hermiticity). Clearly, $\langle\psi_n^r|u\rangle = 0$ yet the signal $|u\rangle$ will excite the state $|\psi_n^r\rangle$. The converse is also

true. An input given by $|u\rangle = |\psi_m^r\rangle$ will excite only the state $|\psi_m^r\rangle$ even though it may have a finite overlap with other states.

Defective spectrum does not mean defective response. We now consider the case when the spectrum of the Hamiltonian \hat{H} contains an EP. For generality, we assume that the EP is of order M , i.e., formed by the coalescence of M eigenstates. Such a Hamiltonian operator is said to be *defective* (i.e., the eigenstates of the Hamiltonian do not form a complete basis). In the literature of non-Hermitian optics, the response of a system described by a defective \hat{H} is sometimes studied using perturbative approaches⁹⁵ (see, for instance, ref. 20). While these perturbative expansions eventually lead to correct conclusions, they complicate the analysis and give the impression that the resultant formulas are only approximations. As we describe below, this is actually not the case. On the contrary, one can use exact, non-perturbative expansions to arrive at the same final results in a straightforward fashion. In this section, we focus on the case when the system exhibits only one EP we discuss the more general case in the Supplementary Material.

To proceed, let us denote the eigenvalue and eigenvector corresponding to an EP by $\Omega_{EP} = \Omega_{EP}^R + i\Omega_{EP}^I$ and $|\psi_{EP}^r\rangle$, respectively. In order to avoid any confusion, we will also refer to the Hamiltonian and its corresponding resolvent in this case by \hat{H}_{EP} and $\hat{G}_{EP}(\omega)$. Note that, since the Hamiltonian \hat{H}_{EP} is defective, $\hat{G}_{EP}(\omega)$ cannot be expressed using a simple expansion similar to that of Eq. (4). Perturbative methods such as Newton-Puiseux series⁹⁵ have been used in the literature to mitigate this problem and obtain an expansion for $\hat{G}_{EP}(\omega)$. What is often overlooked, however, is that even for a defective \hat{H}_{EP} , the operator $(\omega\hat{I} - \hat{H}_{EP})$ can still be invertible. This key observation can tremendously simplify the analysis in many situations. Particularly, when an optical resonator system operates in the passive mode (i.e., no optical gain) or even in active mode below the lasing threshold (i.e., as in amplifiers), the complex eigenvalue lies in the lower half of the complex plane, i.e., $\Omega_{EP}^I < 0$. On the other hand, probing the response of such a system is done by using external excitation that has a real frequency, i.e., along the real axes. In this case, the corresponding eigenvalue of $\hat{G}_{EP}(\omega)$, which is given by $\mu_{EP} = [\omega - (\Omega_{EP}^R + i\Omega_{EP}^I)]^{-1}$, does not diverge even at resonance when $\omega = \Omega_{EP}^R$. As a result, one can evaluate $\hat{G}_{EP}(\omega)$ by direct matrix inversion for any value of the real frequency ω . In principle, this information is sufficient for characterizing the linear response of the resonator, but it does not provide much insight into the interplay between the excitation profile and the response. In addition, one may wonder about the fate of the expansion in (4). As we mentioned earlier, Newton-Puiseux series is often used to generalize this expression. We now show that this generalization is in fact exact and does not employ any perturbation analysis. To do so, we first note that the non-degenerate eigenvectors of an $N \times N$ matrix \hat{G}_{EP} that has an EP of order M span only a reduced $N - M$ dimensional space, call it \mathcal{D}_ϕ . We will denote the missing domain by \mathcal{D}_{EP} . In order to form a complete basis, we follow the standard Jordan chain procedure⁹⁶, defined by the set of vectors that satisfy the following recursive equations:

$$\begin{aligned} (\hat{H}_{EP} - \Omega_{EP}\hat{I})|J_1^r\rangle &= 0 \\ (\hat{H}_{EP} - \Omega_{EP}\hat{I})|J_2^r\rangle &= \chi_2|J_1^r\rangle \\ &\vdots \\ (\hat{H}_{EP} - \Omega_{EP}\hat{I})|J_M^r\rangle &= \chi_M|J_{M-1}^r\rangle. \end{aligned} \tag{5}$$

In the above, we used the notation $|J_1^r\rangle \equiv |\psi_{EP}^r\rangle$ for clarity. The constants χ 's are introduced to ensure the consistency of the physical dimensions, and their values are chosen to achieve normalization, i.e., $\langle J_n^r|J_n^r\rangle = 1$ for any integer $n = 1, 2, \dots, M$. The vectors $|J_n^r\rangle$ are generalized right eigenvectors of the operator \hat{H}_{EP} , i.e., they satisfy the eigenvalue problem $(\hat{H}_{EP} - \Omega_{EP}\hat{I})^n|J_n^r\rangle = 0$ which implies that $\langle \psi_m^l|J_n^r\rangle = 0$ for any n and $\langle \psi_m^l|\neq\langle \psi_m^l|$ (see Supplementary Note 2). Since the vectors $|J_n^r\rangle$ are linearly independent by construction (see Supplementary Note 2 for a brief proof), it follows that they span the domain \mathcal{D}_{EP} , and thus complete the basis. Note, however, that while $|J_1^r\rangle$ is unique (up to a constant), there is a freedom in choosing the set of other vectors $|J_n^r\rangle$ for $n > 1$. Intuitively, this situation is similar to fixing the z axis in three dimensions and rotating the x and y axes in the x - y plane around the origin. Thus, in general extra normalization conditions are required in order to fix the choice of the vectors $|J_n^r\rangle$. Here, we will not be concerned with the exact orientation of $|J_n^r\rangle$. Another important observation is that some of the $|J_n^r\rangle$ vectors are self-orthogonal (see Supplementary Note 2). Thus, while any arbitrary input can be decomposed according to $|u\rangle = \sum_{n=1}^{N-M} c_n|\psi_n^r\rangle + \sum_{m=1}^M d_m|J_m^r\rangle$ with the constants $c_n = \langle \psi_n^l|u\rangle$ evaluated using biorthogonality as before, the coefficients d_m cannot be obtained directly using the same strategy. However, as we show in Supplementary Note 2, one can use the vectors of $(|J_m^l\rangle)$ to define another set of vectors $(|\tilde{J}_m^l\rangle)$ that satisfy the relation $\langle \tilde{J}_m^l|J_n^r\rangle = \delta_{m,n}$ and hence $d_m = \langle \tilde{J}_m^l|u\rangle$.

Next, given the above input signal $|u\rangle$, we seek a similar expansion of the output, i.e., in the form: $\hat{G}_{EP}|u\rangle = \sum_{n=1}^{N-M} \tilde{c}_n|\psi_n^r\rangle + \sum_{m=1}^M \tilde{d}_m|J_m^r\rangle$, or equivalently $(\omega\hat{I} - \hat{H}_{EP})\{\sum_{n=1}^{N-M} \tilde{c}_n|\psi_n^r\rangle + \sum_{m=1}^M \tilde{d}_m|J_m^r\rangle\} = \sum_{n=1}^{N-M} c_n|\psi_n^r\rangle + \sum_{m=1}^M d_m|J_m^r\rangle$. By applying the operator $\omega\hat{I} - \hat{H}_{EP}$ to each term inside the summation and rearranging, we obtain a sum of the form $\sum_{n=1}^{N-M} C_n|\psi_n^r\rangle + \sum_{m=1}^M D_m|J_m^r\rangle = 0$. By noting that all the vectors $|\psi_n^r\rangle$ and $|J_m^r\rangle$ are linearly independent, we find that the above relation can be satisfied if and only if all the coefficients $C_n = D_m = 0$ for every n and m . This finally leads to the expansion (see Supplementary Note 4 for details):

$$\hat{G}_{EP} = \sum_{n=1}^{N-M} \frac{|\psi_n^r\rangle\langle\psi_n^l|}{\omega - \Omega_n} + \sum_{m=1}^M \sum_{k=m}^M \alpha_k^{(m)} \frac{|J_m^r\rangle\langle\tilde{J}_k^l|}{(\omega - \Omega_{EP})^{k-m+1}}, \tag{6}$$

where the coefficients α 's are defined by the recursive relations $\alpha_n^{(m)} = 1$, $\alpha_k^{(m)} = \alpha_{k-1}^{(m)}\chi_k$ for $m < k \leq M$ (see Supplementary Note 4).

We now pause to make several comments on the above expression. First, the expansion series is finite and hence no convergence analysis is needed. Second, due to the same reason (finite terms in the series), its completeness is guaranteed. Importantly, the above expression is exact and non-perturbative despite the fact that the spectrum of \hat{H} contains an EP. Another important observation is that the expansion in Eq. (6) is not unique: a different choice of the vectors $|J_m^r\rangle$ with $m > 1$ will lead to a different series (though more complicated one). Third, unlike previous works that considered small systems⁹⁷, expressions for the resolvent that applies only in the vicinity of EPs⁹⁸ or expansions of the resolvent as a power series of the Hamiltonian itself⁹⁹, the above expansion is valid everywhere in the frequency domain for any system with arbitrary size and is expressed in terms of the eigenvector and canonical vectors. Finally, we emphasize a crucial point: expression (6) for the resolvent is

evaluated for a system “with” an EP not “at” an EP. This semantic difference has caused confusion in the literature, mainly conveying an impression that these systems can be studied only within the context of perturbation analysis. An EP is a characteristic of the system itself, not the probe. The former can contain an EP in its spectrum that lies in the complex plane away from the real axes and still be probed with a signal that has a real frequency to obtain finite response without any singularities or divergences. On the other hand, probing the system at an EP entails either using a probe with complex frequency^{100–102} or supplying enough gain to bring the complex exceptional eigenvalue to the real axis. In both cases, the resolvent will diverge, which corresponds to the fact that the amplitude of the oscillations will grow indefinitely. In reality, however, this does not happen because nonlinear effects regulate the dynamics (think of gain saturation in laser systems for instance).

Super-Lorentzian frequency response. In realistic configurations, a resonant structure interacts with its environment via certain scattering or coupling channels defined by the geometry. One can either probe the system via individual channels or by excitation profiles that are superpositions of several channels. At the abstract level, the concepts of channel and excitation profile are the same since they are just related by unitary transformations. In this section, we will focus on channels that directly excite the vectors $|\psi_n^r\rangle$ and $|J_m^r\rangle$ and analyze their scattering/coupling characteristics. We begin by rewriting the expression in Eq. (6) after unfolding the double summation:

$$\hat{G}_{EP}(\omega) = \sum_{n=1}^{N-M} \frac{|\psi_n^r\rangle\langle\psi_n^r|}{\omega - \Omega_n} + \sum_{k=1}^M \frac{\alpha_k^{(1)} |J_1^r\rangle\langle J_k^r|}{(\omega - \Omega_{EP})^k} + \sum_{k=2}^M \frac{\alpha_k^{(2)} |J_2^r\rangle\langle J_k^r|}{(\omega - \Omega_{EP})^{k-1}} + \dots + \frac{|J_M^r\rangle\langle J_M^r|}{\omega - \Omega_{EP}}. \tag{7}$$

Clearly, an input signal with a profile $|u\rangle = |\psi_n^r\rangle$ will only excite the mode $|\psi_n^r\rangle$ with a Lorentzian response centered at Ω_n as expected. Similarly, an input that matches the exceptional vector $|u\rangle = |J_1^r\rangle$ will excite only the mode $|J_1^r\rangle$, also with a Lorentzian response. A more interesting situation arises when the excitation profile coincides with a higher-order Jordan vector, say $|u\rangle = |J_k^r\rangle$. In that case, according to Eq. (7), the exceptional eigenvector will be excited with a frequency response that features an k th order super-Lorentzian lineshape (i.e., a Lorentzian function raised to the power k). In addition, each of the states $|J_m^r\rangle$ with $1 < m \leq k$ (which are not eigenstates of \hat{H}_{EP}) will be also excited with a frequency response that corresponds to a super-Lorentzian of order $k - m + 1$. At this point, it is important to reiterate our previous comment on the freedom of choosing the set $|J_m^r\rangle$. While $|J_1^r\rangle$ is unique, the vectors $|J_m^r\rangle$, $1 < m \leq M$ are not. The consequences of this observation are not trivial. For instance, in order to excite the exceptional vector with a certain super-Lorentzian response, one can choose from a continuous manifold of excitation profiles. To illustrate this, we consider the excitation of $|J_1^r\rangle$ with a second-order super-Lorentzian response. This can be done by using the input $|u\rangle = |J_2^r\rangle + x|J_1^r\rangle$, where x is a free parameter. We anticipate that these general results, which are illustrated schematically in Fig. 5b, will be instrumental in developing a more comprehensive understanding of the quantum limits of several non-Hermitian optical devices (such as lasers, amplifiers, and sensors) operating at EPs. Equally important, the above analysis provides a complete picture of how the frequency response of non-Hermitian systems with EPs scales as a function

of the input profile, which can be of great utility in engineering devices that rely on this feature, such as optical amplifiers with relaxed gain-bandwidth restrictions^{29,103}. In addition, our analysis can be also used to classify the input channel according to their interference effects inside the resonant system as we explain in detail in Supplementary Notes 5 and 6. Finally, we note that, so far we have focused on situations where the system has only one EP. Supplementary Note 7 discusses the case when the spectrum of the relevant Hamiltonian has multiple EPs.

Connection with experiments. Here we present illustrative realistic examples that demonstrate some of the results discussed in this work as well as the power and insight provided by our formalism which expresses the resolvent operator as an exact expansion series of the right/left canonical vectors.

Our first example is depicted in Fig. 6a. It consists of a microring resonator evanescently coupled to two identical waveguides, with one port of, say, W_1 terminated by a mirror. This geometry was introduced in ref. ²³ and shown to exhibit an exceptional surface with potential applications for sensing and controlling spontaneous emission³¹. In addition, it has been recently implemented using an on-chip microsphere resonator with the feedback realized using a fiber loop mirror¹⁰⁴. It is described by the following set of equations:

$$i \frac{d}{dt} \begin{bmatrix} a_1(t) \\ a_2(t) \end{bmatrix} = \begin{bmatrix} \omega_o - 2i\gamma & 0 \\ \kappa & \omega_o - 2i\gamma \end{bmatrix} \begin{bmatrix} a_1(t) \\ a_2(t) \end{bmatrix} + i\sqrt{2\gamma} \begin{bmatrix} b_1(t) \\ b_2(t) \end{bmatrix} \tag{8}$$

$$Q_1 = -\sqrt{2\gamma} a_2$$

$$Q_2 = P_1 - \sqrt{2\gamma} a_2,$$

where, ω_o is the resonant frequency, γ is the decay rate of the resonant mode into each waveguide. In addition, $\kappa = -2i\gamma|r|e^{i\phi}$, where $|r|$ is the absolute value of the mirror amplitude reflection coefficient, and $\phi \equiv 2\beta L + \phi_r$ is a phase factor that quantifies the phase of the mirror reflectivity, ϕ_r , and its distance from the resonator, L , where β is the propagation constant in the waveguide.

The resolvent in this case, which we will denote by G_2 can be evaluated in closed form and is given by:

$$G_2(\omega) = \begin{bmatrix} \frac{1}{\Delta\omega + 2i\gamma} & 0 \\ \frac{\kappa}{(\Delta\omega + 2i\gamma)^2} & \frac{1}{\Delta\omega + 2i\gamma} \end{bmatrix}, \tag{9}$$

where $\Delta\omega = \omega - \omega_o$. It is straightforward to show that $|\psi_{EP}^r\rangle \equiv |J_1^r\rangle = [0, 1]^T$ and $|J_2^r\rangle = \frac{x}{\kappa}[1, 0]^T$. Note that $\langle J_1^r | J_1^r \rangle = 1$, while $\langle J_2^r | J_2^r \rangle \neq 1$, i.e., the latter is not normalized. If we now consider the two normalized inputs $|b_{1,2}\rangle = \alpha_{1,2} |J_{1,2}^r\rangle e^{-i\omega t}$ with $\alpha_1 = 1$ and $\alpha_2 = \frac{x}{\kappa}$ we find that the normalized stored energies are given by $\langle E_1 \rangle = \frac{2\gamma}{\Delta\omega^2 + 4\gamma^2}$ and $\langle E_2 \rangle = \frac{2\gamma}{\Delta\omega^2 + 4\gamma^2} \left[1 + \frac{4\gamma^2 |r|^2}{\Delta\omega^2 + 4\gamma^2} \right]$. Thus, $\eta \equiv \frac{\langle E_2 \rangle}{\langle E_1 \rangle} = 1 + \frac{4\gamma^2 |r|^2}{\Delta\omega^2 + 4\gamma^2} > 1$. At resonance when $\Delta\omega = 0$, we find that $\eta = 2$ when a completely reflecting mirror, $r = 1$, is used.

To confirm these predictions, we consider a realistic photonic implementation of the structure of Fig. 6a as explained in detail in Supplementary Note 8. It is straightforward to show that excitations from ports $P_{1,2}$ are mode-matched with $|J_{1,2}^r\rangle$, respectively. Figure 6b plots the value of η as a function of the frequency detuning as obtained from the full-wave simulations (black dots) as well as by direct substitution in the closed-form expression for η described above (red line). On the other hand, Fig. 6c, d depicts the steady-state field distribution as obtained by full-wave analysis (see Supplementary Note 8 for the details of the optical parameters of the structure used in the simulations) inside the system under the two different excitations at resonance. In

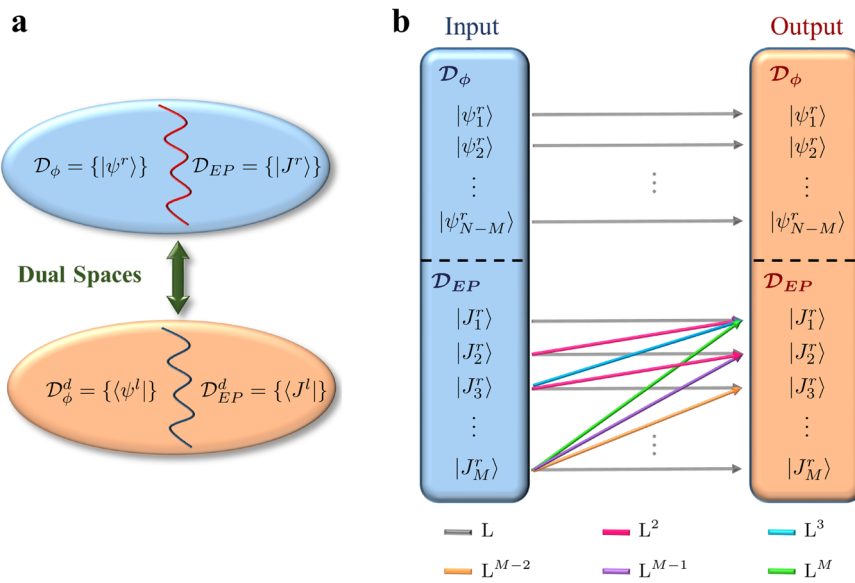


Fig. 5 Structure of the eigenspace and its fingerprint on the linear response. **a** The underlying vector space associated with the non-Hermitian Hamiltonian \hat{H} can be divided into two subspaces: $\mathcal{D}_\phi = \{|\psi_n^r\rangle : n = 1, 2, \dots, N - M\}$ and $\mathcal{D}_{EP} = \{|\psi_m^l\rangle : m = 1, 2, \dots, M\}$. The former is spanned by the non-degenerate right eigenvectors of \hat{H} , while the latter is spanned by the right generalized eigenvectors. Note that in this classification, the degenerate (or exceptional) vector belongs to \mathcal{D}_{EP} . The dual spaces \mathcal{D}_ϕ^d and \mathcal{D}_{EP}^d are defined in a similar fashion for the left ordinary and generalized eigenvectors. **b** Pictorial representation of the linear response associated with a non-Hermitian system having an EP. Typical Lorentzian response arises due to coupling between an input and an output channel that belong to the same modal class. On the other hand, super-Lorentzian responses emerge when the input signal matches a particular generalized eigenmodes of certain order while the output signal matches a lower order generalized eigenvector (including the exceptional vector) according to Eq. (6). The arrows, together with the legends, illustrate a few possible responses explicitly. The symbol L^m indicates a super-Lorentzian response of order m , i.e., a Lorentzian raised to the power m .

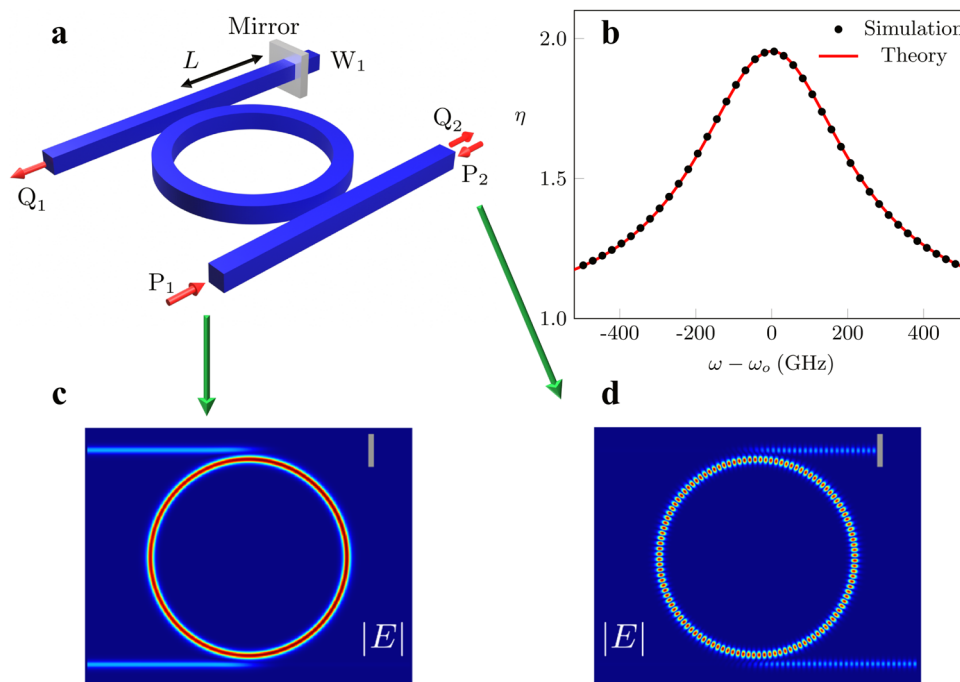


Fig. 6 Optical energy inside a photonic resonator with a second-order EP. **a** A schematic of a photonic structure that exhibits a second-order EP: it consists of a microring resonator evanescently coupled to two identical waveguides, one of which is terminated with a mirror at port W_1 . The exceptional eigenstate $|J_1^r\rangle = |\psi_{EP}^r\rangle$ can be excited through port P_1 , while the generalized eigenstate $|J_2^r\rangle$ can be excited via port P_2 . **b** Plot of η (enhancement factor of stored energy in the microring) when the system is excited by an input that matches $|J_2^r\rangle$ compared to an excitation matching $|\psi_{EP}^r\rangle$ as a function of frequency detuning near resonance as obtained by full-wave simulations (black dots) and the closed-form expression (red line). **c, d** Distributions of the electric field amplitudes under excitation either from ports P_1 or P_2 are plotted. As expected from the analysis, the case when $|u_1\rangle = |\psi_{EP}^r\rangle$ leads to energy storage in both the CW and CCW modes as evidenced by the standing wave pattern in **(d)**. All simulations were performed by using the finite element method available from the COMSOL software package. The optical parameters of the structure and the simulations details are discussed in Supplementary Note 8.

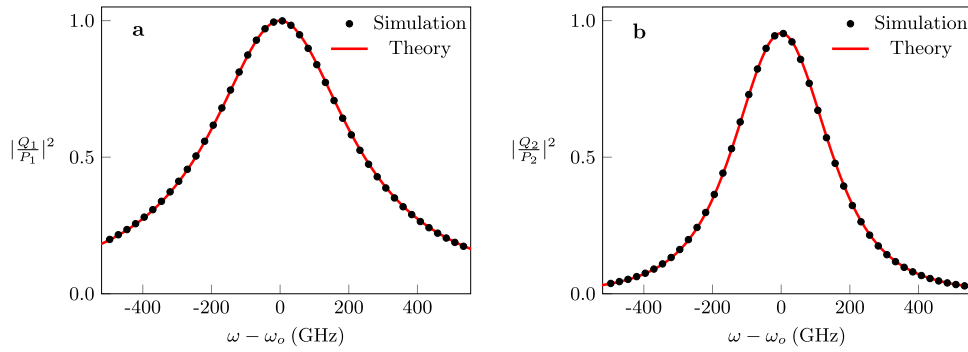


Fig. 7 Illustration of the Lorentzian and square-Lorentzian responses of the system. **a** An input signal is launched from port P_1 (see Fig. 6a) and the normalized output power $|\frac{Q_1}{P_1}|^2$ with Lorentzian distribution is observed at port Q_1 . **b** For an input signal from port P_2 a square-Lorentzian response for the normalized output power $|\frac{Q_2}{P_2}|^2$ is collected at port Q_2 . Red solid line shows the theoretical results while black dots show results obtained through simulations.

order to study the spectral response of this configuration, we plot the scattering coefficients $|\frac{Q_1}{P_1}|^2$ and $|\frac{Q_2}{P_2}|^2$ in Fig. 7a, b, where the black dots represent data obtained from full-wave simulations and red line indicates theoretical results. As predicted by our analysis [see Eq. (8)], $|\frac{Q_1}{P_1}|^2$ which corresponds to an excitation and collection from the exceptional vector features a Lorentzian response, while $|\frac{Q_2}{P_2}|^2$ which corresponds to an excitation matching $|J_2^r\rangle$ and collection matching $|\psi_{EP}^r\rangle$ follows a super-Lorentzian of order two. This simple but intuitive example demonstrates a subtle property of open systems, namely that their response lineshape is not unique but rather depends on the input/output channel configuration. Not only this feature arises naturally from our analysis, but the exact expansion series for resolvent operator [see Eq. (6)] allows us to tailor this response at will by selecting the appropriate coupling channels. Importantly, we stress that this scenario is different from the previous works in which a control parameter, such as coupling strength, frequency detuning, or loss imbalance between resonance modes, is tuned to feature a Fano, EIT, or an ATS lineshape^{105–108}. In contrast, for the system studied here, there is no such control parameter: one can obtain a Lorentzian or a squared-Lorentzian lineshape by choosing the appropriate input and output channel pairs.

Our analysis extends beyond the simple input/output evanescently coupled channels and can be useful also in understanding light-matter interaction at EPs. As an example, consider the geometry depicted in Fig. 8a which consists of a quantum dot embedded inside a microring-waveguide-mirror system implementing an exceptional surface. This system was investigated recently and it was shown that it can be used to control the rate of spontaneous emission and Purcell factor^{31,36,77}. Let us now assume that two single-photon detectors, $D_{1,2}$ are located as shown in the figure. What would be the spectrum of the detected photon as measured by each detector after repeating the experiment a large number of times? This question can be answered only by calculating the Green's operator matrix elements. While this task can be done easily by a matrix inversion in this simple case (see ref. 31 for more details), this approach does not give any insight into the physics of the system. On the other hand, by applying our formalism, it is straightforward to see, based on the photon trajectories, that detector D_1 will report a Lorentzian response while D_2 will report a superposition of Lorentzian and super-Lorentzian of order two. More rigorously, the system here is described by equations similar to that presented in Eq. (8) (see ref. 31 for details), where here $|b_{1,2}\rangle$ represent the emission from the quantum dot and are given by: $[b_1(t), b_2(t)]^T = \frac{J_e e^{-i\omega_e t}}{i\sqrt{2}\gamma} [e^{-i\phi_E}, e^{i\phi_E}]^T$, where ω_e is the transition

frequency of the QE, the phase $\phi_E = \beta d$, and β is the propagation constant of the modes (see ref. 31 for a detailed derivation). By using the resolvent in Eq. (9), the response of the system is calculated as: $G_2(\omega_e)[J_e e^{-i\phi_E}, J_e e^{i\phi_E}]^T = \frac{J_e}{\Delta\omega + 2i\gamma} [e^{-i\phi_E}, e^{i\phi_E} + \frac{\kappa}{\Delta\omega + 2i\gamma} e^{-i\phi_E}]^T$. The above expression indicates that the power spectrum of CW mode associated with the microring structure in Fig. 8a is Lorentzian while that of the CCW mode features a superposition of Lorentzian and square-Lorentzian terms. In addition, by recalling that κ is a function of the mirror reflectivity and location, it is straightforward to see that the interference effects associated with the mixed term will vary as a function of the optical path between the mirror and the emitter $\Delta\phi \equiv 2\phi_E - \phi = 2\beta(d - L) + \phi_r$. Figure 8b depicts the ratio of the stored energy in the CCW mode to that in the CW mode $\eta_c \equiv \frac{\langle E_2 \rangle}{\langle E_1 \rangle} = |1 - \frac{2i\gamma|r|e^{-i\Delta\phi}}{\Delta\omega + 2i\gamma}|^2$ as a function of the mirror reflectivity $|r|$ and $\Delta\phi$, which clearly highlights how the response of the intra-cavity modes depends on the relative position of the mirror with respect to the emitter. For completeness, we also plot the normalized output power spectra $P_{D_{1,2}} = |\frac{\sqrt{2}\gamma Q_{1,2}}{J_e}|^2$ detected by $D_{1,2}$ as a function of the normalized frequency detuning $\frac{\Delta\omega}{\gamma}$ as shown in Fig. 8c, d, respectively. As expected, $P_{D_1} = \frac{4\gamma^2}{\Delta\omega^2 + 4\gamma^2}$ is Lorentzian, while $P_{D_2} = \frac{4\gamma^2}{\Delta\omega^2 + 4\gamma^2} |1 - \frac{2i\gamma|r|e^{-i\Delta\phi}}{\Delta\omega + 2i\gamma}|^2$ features an interference between a Lorentzian and square-Lorentzian terms. While the above example considers realistic scenarios of a quantum dot having a small size compared to the wavelength of light, the notion of controlling spontaneous emission using exceptional points could be also relevant to other setups involving artificial atoms with larger size where the dipole approximation fails¹⁰⁹, as well as systems consisting of multiple quantum emitters¹¹⁰.

Having demonstrated the utility of our approach and the insight it provides using a simple system with one resonant element, we now consider a more complex system that consists of a PT-symmetric arrangement and an asymmetric delayed feedback as shown in Fig. 9a. In the absence of the mirror, this structure exhibits two independent EPs, each of which of order two. The introduction of the mirror causes these two EPs to coalesce, forming an EP of order four³⁰. Despite the fact that this system consists of only two ring resonators, the presence of inhomogeneous gain and loss distribution makes it difficult to trust intuition in this case. On the other hand, brute-force analysis by evaluating the scattering coefficients one at a time does not provide much insight into the scattering profile. To analyze this system using our formalism, we first consider the

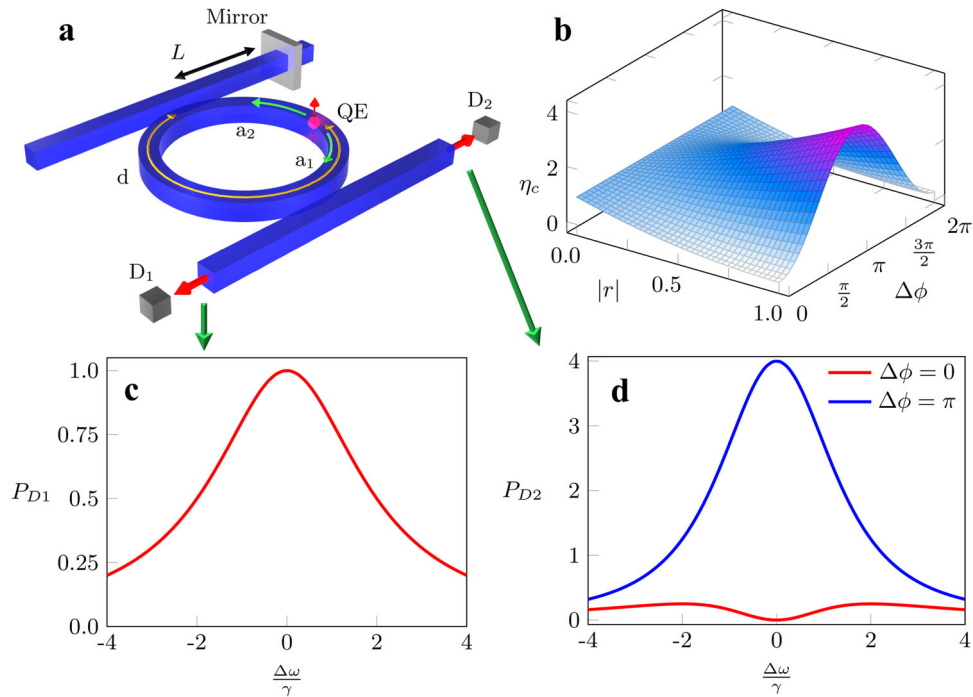


Fig. 8 Spontaneous emission at exceptional surfaces. **a** A photonic system consisting of a quantum dot embedded in a microring resonator evanescently coupled to a waveguide with an end mirror that induces a unidirectional coupling between these modes. The emission from the quantum dot couples to the CW and CCW modes ($a_{1,2}$) of the ring and eventually detected by the detectors $D_{1,2}$. **b** The ratio η_c of the stored energy in the CCW mode to the stored energy in the CW wave is plotted for the resonant frequency $\omega = \omega_o$. **c** The normalized power detected by D_1 has a Lorentzian distribution. **d** The normalized power detected by D_2 for $\Delta\phi = 0$ (red curve) and $\Delta\phi = \pi$ (blue curve) are shown for $|r|=1$. As explained in the text, the detected power spectrum at D_2 features an interference between a Lorentzian and a square-Lorentzian terms, with the final outcome strongly depending on the relative position between the mirror and the quantum dot as quantified by the parameter $\Delta\phi$.

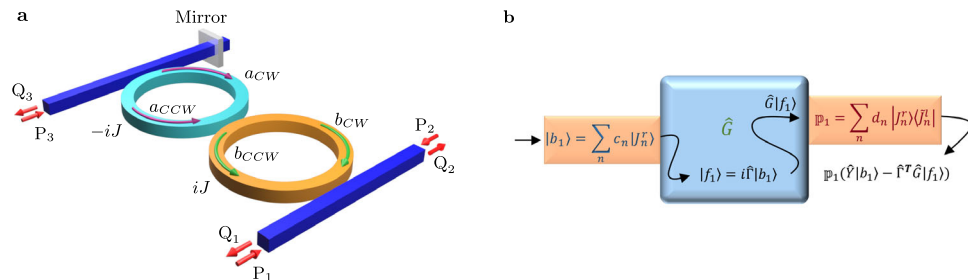


Fig. 9 A PT-symmetric system with unidirectional coupling between the CW/CCW modes. **a** A schematic of the studied system, which was introduced in ref. 30 and shown to exhibit an EP of order 4. J is the gain/loss factor. $P_{1,2,3}$ are input signals and $Q_{1,2,3}$ are output signals. $a_{CW,CCW}$ and $b_{CW,CCW}$ are CW and CCW modes of the cavities. **b** Pictorial depiction of the systematic approach to obtain the system's linear response using the formalism presented in this work. $|b_1\rangle$ is the excitation profile expanded with respect to the right eigenvectors $\{|J_n^r\rangle\}$. $\{\langle J_n^l|\}$ are the corresponding left bi-orthogonal vectors. \hat{G} is the resolvent and \mathbb{P}_1 is the projection operator assigned to the output channel. \hat{Y} quantifies the direct scattering between incoming and outgoing channels and $\hat{\Gamma}$ describes the coupling between the resonant modes and the input/output channels.

Hamiltonian matrix describing this system as written in the natural basis of the individual, isolated ring resonators $[a_{CW}, b_{CCW}, a_{CCW}, b_{CW}]^T$:

$$\hat{H}_4 = \begin{bmatrix} \omega_o - i\gamma - iJ & J & 0 & 0 \\ J & \omega_o - i\gamma + iJ & 0 & 0 \\ \kappa & 0 & \omega_o - i\gamma - iJ & J \\ 0 & 0 & J & \omega_o - i\gamma + iJ \end{bmatrix}, \tag{10}$$

Here, ω_o is the resonant frequency, γ is the decay rate of the resonant mode into each waveguide, J is the coupling rate between the two rings and also the gain/loss factors in the yellow/green rings, respectively, i.e., the system respects PT symmetry. In

addition, $\kappa = -2i\gamma|r|e^{i\phi}$, where $|r|$ is the absolute value of the mirror reflection coefficient, and the phase factor ϕ quantified the phase of the mirror reflection coefficient and its distance from the adjacent resonator. The right (canonical) eigenvectors associated with this Hamiltonian are given $|J_1^r\rangle = [0, 0, -i, 1]^T$, $|J_2^r\rangle = [0, 0, 1, 0]^T$, $|J_3^r\rangle = [1, i, 0, 0]^T$, and $|J_4^r\rangle = [0, 1, 0, 0]^T$. These vectors are calculated based on the following choice for constant coefficients χ^s [see Eq. (5)]: $\chi_2 = \chi_4 = J, \chi_3 = \kappa$. The corresponding left bi-orthogonal vectors, which satisfy the relation $\langle J_n^l | J_m^r \rangle = \delta_{nm}$, are then given by: $\langle J_1^l | = [-i, 1, 0, 0]$, $\langle J_2^l | = [1, 0, 0, 0]$, $\langle J_3^l | = [1, i, 0, 0]$, and $\langle J_4^l | = [0, 0, 0, 1]$. The scattering profile and spectral response of the system can be

then evaluated by using Eq. (6) and using the following systematic steps: (1) Write down the excitation profile in the basis of the bare eigenmodes a_{CW} , a_{CCW} , b_{CW} , and b_{CCW} ; (2) Express this vector in the basis of the right (canonical) eigenvectors; (3) Obtain the response using Eq. (6); (4) Assign a projection operator to each output channel. For instance, a unit input signal from port P_1 will directly couple only to the field amplitude b_{CCW} (see Fig. 9a), and hence we have the input vector $|b_1\rangle = [0, 1, 0, 0]^T = |J_4^r\rangle$. Similarly, the vectors $|b_2\rangle = [0, 0, 0, 1]^T = |J_1^r\rangle + i|J_2^r\rangle$ and $|b_3\rangle = [1, 0, 0, 0]^T = |J_3^r\rangle - i|J_4^r\rangle$ correspond to unit input signals from ports P_2 and P_3 , respectively. By using Eq. (6), we can now obtain the Green's operator, and hence the linear response for each different excitation. For instance, in the case of P_1 , we obtain $G_4(\omega)|f_1\rangle = G_4(\omega)\hat{\Gamma}|b_1\rangle = i\sqrt{2\gamma}\left[\frac{J^k}{(\Delta\omega+i\gamma)^4}|J_1^r\rangle + \frac{Jk}{(\Delta\omega+i\gamma)^3}|J_2^r\rangle + \frac{J}{(\Delta\omega+i\gamma)^2}|J_3^r\rangle + \frac{1}{(\Delta\omega+i\gamma)}|J_4^r\rangle\right]$, where $|f_1\rangle = \hat{\Gamma}|b_1\rangle$ and $\sqrt{2\gamma}$ corresponds to the element of the coupling matrix $\hat{\Gamma}$ between the input channels and the interior of the resonator system. Note that this expression describes the field amplitude inside the resonators. To calculate the output, one must project this field amplitude on the output channel. For illustration purpose, let us consider the output channel Q_1 , which is directly coupled to the b_{CW} , i.e., it corresponds to the vector $[0, 0, 0, 1]^T = |J_1^r\rangle + i|J_2^r\rangle$. Thus one can assign the projection operator $\mathbb{P}_1 = |J_1^r\rangle\langle J_1^r| + i|J_2^r\rangle\langle J_2^r|$ to the output channel Q_1 . Similarly, the projection operators $\mathbb{P}_2 = |J_4^r\rangle\langle J_4^r|$ and $\mathbb{P}_3 = |J_2^r\rangle\langle J_2^r|$ describe output channels Q_2 and Q_3 , respectively. Finally, the output signal is given by: $\mathbb{P}_i[\hat{Y}|b_j\rangle - \hat{\Gamma}^T\hat{G}|f_j\rangle]$, where the matrix \hat{Y} quantifies the direct coupling between the input and output channels whereas the matrix $\hat{\Gamma}^T$ describes the coupling between the interior of the resonators and the output channels. By applying the above-sketched recipe for an input/output from ports P_1 and Q_3 , we find: $Q_3 = -i\frac{2\gamma Jk}{(\Delta\omega+i\gamma)^2}$. In other words, counter-intuitively the response features a super-Lorentzian of order three, despite the fact that the system exhibits an EP of order four. This is, however, fully consistent with our theoretical analysis since P_1 corresponds to $|J_4^r\rangle$ and Q_3 corresponds to $|J_2^r\rangle$ as demonstrated by mathematical structure of Eq. (6), and also pictorially in Fig. 5b. Figure 9b summarizes the steps described in this section.

Discussion

In this work, we have presented a detailed analysis of the linear response associated with non-Hermitian systems having EPs and showed that a non-diverging resolvent associated with the system's Hamiltonian can be expressed as an exact series expansion of the ordinary and generalized eigenfunctions of the Hamiltonian, i.e., without resorting to any perturbation approximation. Importantly, our formalism revealed a feature that escaped attention in previous studies, namely that the response lineshape scaling can be engineered by a judicious choice of the input and output channels. This observation is crucial for tailoring light-matter interactions at EPs. In order to emphasize this point and also clarify the application of our formalism, we have considered and analyzed several realistic photonic examples and we found excellent agreement between results obtained from full-wave simulations and our formulas. In doing so, we have also demonstrated an interesting effect analogous to adjoint coupling but rather in microring cavity setups. In other words, we have shown that more optical energy can be stored in a microring cavity system having an EP when the channel associated with the input signal matches the generalized eigenmode rather than the

actual ordinary eigenmode of the structure. We emphasize that although the examples in this manuscript are chosen from the optical domain, our results are general and applicable to other physical systems that can be described by similar coupled-mode formalism. These include electronic, acoustic, mechanical, and thermal systems. In addition, our framework provides a powerful tool for understanding the complex interplay between non-Hermiticity and other physical effects such as topological invariants^{12,28,55,65,111,112}, optomechanical coupling^{14,54,113–115} as well as quantum statistics^{10,24,72,103,116,117}, to just mention a few examples. This in turn may enable the engineering of more elaborate schemes for controlling energy and information flow in complex non-Hermitian systems. Finally, we remark that understanding the linear response of non-Hermitian systems is a very crucial step toward studying their noise. In this regard, we expect our formalism to provide more insight into the noise behavior in non-Hermitian systems and play a positive role in the active debate on signal-to-noise ratio of EP-based sensors^{118–124}. We plan to explore some of these interesting directions in future works.

Data availability

The data that support the findings of this study are available from the corresponding authors upon reasonable request.

Received: 19 July 2021; Accepted: 12 May 2022;

Published online: 07 June 2022

References

- Vahala, K. J. Optical microcavities. *Nature* **424**, 839–846 (2003).
- Gramotnev, D. K. & Bozhevolnyi, S. I. Plasmonics beyond the diffraction limit. *Nat. Photon.* **4**, 83–91 (2010).
- Petermann, K. Calculated spontaneous emission factor for double-heterostructure injection lasers with gain-induced waveguiding. *IEEE J. Quantum Electron.* **15**, 566–570 (1979).
- Siegman, A. E. Excess spontaneous emission in non-Hermitian optical systems. I. Laser amplifiers. *Phys. Rev. A* **39**, 1253–1263 (1989).
- El-Ganainy, R., Makris, K. G., Christodoulides, D. N. & Musslimani, Z. H. Theory of coupled optical PT-symmetric structures. *Opt. Lett.* **32**, 2632–2634 (2007).
- Musslimani, Z. H., Makris, K. G., El-Ganainy, R. & Christodoulides, D. N. Optical solitons in PT periodic potentials. *Phys. Rev. Lett.* **100**, 030402 (2008).
- Makris, K. G., El-Ganainy, R., Christodoulides, D. N. & Musslimani, Z. H. Beam dynamics in PT symmetric optical lattices. *Phys. Rev. Lett.* **100**, 103904 (2008).
- Guo, A. et al. Observation of PT-symmetry breaking in complex optical potentials. *Phys. Rev. Lett.* **103**, 093902 (2009).
- Ruter, C. E. et al. Observation of parity-time symmetry in optics. *Nat. Phys.* **6**, 192–195 (2010).
- Schomerus, H. Quantum noise and self-sustained radiation of PT-symmetric systems. *Phys. Rev. Lett.* **104**, 233601 (2010).
- Wiersig, J. et al. Nonorthogonal pairs of copropagating optical modes in deformed microdisk cavities. *Phys. Rev. A* **84**, 023845 (2011).
- Schomerus, H. Topologically protected midgap states in complex photonic lattices. *Opt. Lett.* **38**, 1912–1914 (2013).
- Schomerus, H. & Wiersig, J. Non-Hermitian-transport effects in coupled-resonator optical waveguides. *Phys. Rev. A* **90**, 053819 (2014).
- Jing, H. et al. PT-symmetric phonon laser. *Phys. Rev. Lett.* **113**, 053604 (2014).
- Wiersig, J. Enhancing the sensitivity of frequency and energy splitting detection by using exceptional points: application to microcavity sensors for single-particle detection. *Phys. Rev. Lett.* **112**, 203901 (2014).
- Zhong, Q., Ahmed, A., Dadap, J. I., JR, R. M. O. & El-Ganainy, R. Parametric amplification in quasi-PT symmetric coupled waveguide structures. *New J. Phys.* **18**, 125006 (2016).
- Wiersig, J. Sensors operating at exceptional points: general theory. *Phys. Rev. A* **93**, 033809 (2016).
- Lin, Z., Pick, A., Loncar, M. & Rodriguez, A. W. Enhanced spontaneous emission at third-order Dirac exceptional points in inverse-designed photonic crystals. *Phys. Rev. Lett.* **117**, 107402 (2016).

19. Lü, H., Özdemir, S. K., Kuang, L.-M., Nori, F. & Jing, H. Exceptional points in random-defect phonon lasers. *Phys. Rev. Appl.* **8**, 044020 (2017).
20. Pick, A. et al. General theory of spontaneous emission near exceptional points. *Opt. Express* **25**, 12325–12348 (2017).
21. Zhong, Q., Khajavikhan, M., Christodoulides, D. N. & El-Ganainy, R. Winding around non-Hermitian singularities. *Nat. Commun.* **9**, 4808 (2018).
22. Jiang, Y., Maayani, S., Carmon, T., Nori, F. & Jing, H. Nonreciprocal phonon laser. *Phys. Rev. Appl.* **10**, 064037 (2018).
23. Zhong, Q. et al. Sensing with exceptional surfaces in order to combine sensitivity with robustness. *Phys. Rev. Lett.* **122**, 153902 (2019).
24. Arkhipov, I. I. et al. Scully-lamb quantum laser model for parity-time-symmetric whispering-gallery microcavities: Gain saturation effects and nonreciprocity. *Phys. Rev. A* **99**, 053806 (2019).
25. Bliokh, K. Y., Leykam, D., Lein, M. & Nori, F. Topological non-Hermitian origin of surface Maxwell waves. *Nat. Commun.* **10**, 580 (2019).
26. Franke, S. et al. Quantization of quasinormal modes for open cavities and plasmonic cavity quantum electrodynamics. *Phys. Rev. Lett.* **122**, 213901 (2019).
27. Rivero, J. D. H. & Ge, L. Time-reversal-invariant scaling of light propagation in one-dimensional non-Hermitian systems. *Phys. Rev. A* **100**, 023819 (2019).
28. Reséndiz-Vázquez, P., Tschernig, K., Perez-Leija, A., Busch, K. & León-Montiel, R. J. Topological protection in non-Hermitian haldane honeycomb lattices. *Phys. Rev. Res.* **2**, 013387 (2020).
29. Zhong, Q., Özdemir, S., Eisfeld, A., Metelmann, A. & El-Ganainy, R. Exceptional-point-based optical amplifiers. *Phys. Rev. Appl.* **13**, 014070 (2020).
30. Zhong, Q., Kou, J., Özdemir, S. K. & El-Ganainy, R. Hierarchical construction of higher-order exceptional points. *Phys. Rev. Lett.* **125**, 203602 (2020).
31. Zhong, Q., Hashemi, A., Özdemir, S. K. & El-Ganainy, R. Control of spontaneous emission dynamics in microcavities with chiral exceptional surfaces. *Phys. Rev. Res.* **3**, 013320 (2021).
32. Tzortzakakis, A. F., Makris, K. G. & Economou, E. N. Non-Hermitian disorder in two-dimensional optical lattices. *Phys. Rev. B* **101**, 014202 (2020).
33. Komis, I., Sardelis, S., Musslimani, Z. H. & Makris, K. G. Equal-intensity waves in non-Hermitian media. *Phys. Rev. E* **102**, 032203 (2020).
34. Tzortzakakis, A. F., Makris, K. G., Rotter, S. & Economou, E. N. Shape-preserving beam transmission through non-Hermitian disordered lattices. *Phys. Rev. A* **102**, 033504 (2020).
35. Kristensen, P. T., Herrmann, K., Intravaia, F. & Busch, K. Modeling electromagnetic resonators using quasinormal modes. *Adv. Opt. Photon.* **12**, 612–708 (2020).
36. Khanbekyan, M. & Wiersig, J. Decay suppression of spontaneous emission of a single emitter in a high- q cavity at exceptional points. *Phys. Rev. Res.* **2**, 023375 (2020).
37. Hadad, Y. & Engheta, N. Possibility for inhibited spontaneous emission in electromagnetically open parity-time-symmetric guiding structures. *Proc. Natl. Acad. Sci. USA* **117**, 5576–5581 (2020).
38. Hashemi, A., Rezaei, S. M., Özdemir, S. K. & El-Ganainy, R. New perspective on chiral exceptional points with application to discrete photonics. *APL Photonics* **6**, 040803 (2021).
39. Rivero, J. D. H., Pan, M., Makris, K. G., Feng, L. & Ge, L. Non-hermiticity-governed active photonic resonances. *Phys. Rev. Lett.* **126**, 163901 (2021).
40. Feng, L. et al. Experimental demonstration of a unidirectional reflectionless parity-time metamaterial at optical frequencies. *Nat. Mater.* **12**, 108–113 (2013).
41. Peng, B. et al. Parity-time-symmetric whispering-gallery microcavities. *Nat. Phys.* **10**, 394–398 (2014).
42. Hodaei, H., Miri, M.-A., Heinrich, M., Christodoulides, D. N. & Khajavikhan, M. Parity-time-symmetric microring lasers. *Science* **346**, 975–978 (2014).
43. Feng, L., Wong, Z. J., Ma, R.-M., Wang, Y. & Zhang, X. Single-mode laser by parity-time symmetry breaking. *Science* **346**, 972–975 (2014).
44. Chang, L. et al. Parity-time symmetry and variable optical isolation in active-passive-coupled microresonators. *Nat. Photon.* **8**, 524–529 (2014).
45. Peng, B. et al. Loss-induced suppression and revival of lasing. *Science* **346**, 328–332 (2014).
46. Brandstetter, M. et al. Reversing the pump dependence of a laser at an exceptional point. *Nat. Commun.* **5**, 4034 (2014).
47. Gao, T. et al. Observation of non-Hermitian degeneracies in a chaotic exciton-polariton billiard. *Nature* **526**, 554–558 (2015).
48. Zhen, B. et al. Spawning rings of exceptional points out of Dirac cones. *Nature* **525**, 354–358 (2015).
49. Peng, B. et al. Chiral modes and directional lasing at exceptional points. *PNAS* **113**, 6845–6850 (2016).
50. Xu, H., Mason, D., Jiang, L. & Harris, J. G. E. Topological energy transfer in an optomechanical system with exceptional points. *Nature* **537**, 80–83 (2016).
51. Doppler, J. et al. Dynamically encircling an exceptional point for asymmetric mode switching. *Nature* **537**, 76–79 (2016).
52. Chen, W., Özdemir, S. K., Zhao, G., Wiersig, J. & Yang, L. Exceptional points enhance sensing in an optical microcavity. *Nature* **548**, 192–196 (2017).
53. Yoon, J. W. et al. Time-asymmetric loop around an exceptional point over the full optical communications band. *Nature* **562**, 86–90 (2018).
54. Zhang, J. et al. A phonon laser operating at an exceptional point. *Nat. Photon.* **12**, 479–484 (2018).
55. Zhao, H. et al. Topological hybrid silicon microlasers. *Nat. Commun.* **9**, 1–6 (2018).
56. Lai, Y.-H., Lu, Y.-K., Suh, M.-G., Yuan, Z. & Vahala, K. Observation of the exceptional-point-enhanced Sagnac effect. *Nature* **576**, 65–69 (2019).
57. Chen, H.-Z. et al. Revealing the missing dimension at an exceptional point. *Nat. Phys.* **16**, 571–578 (2020).
58. Xia, S. et al. Nonlinear tuning of PT symmetry and non-Hermitian topological states. *Science* **372**, 72–76 (2021).
59. El-Ganainy, R., Makris, K., Khajavikhan, Z. H., Rotter, S. & Christodoulides, D. N. Non-Hermitian physics and PT symmetry. *Nat. Phys.* **14**, 11–19 (2018).
60. Feng, L., El-Ganainy, R. & Ge, L. Non-Hermitian photonics based on parity-time symmetry. *Nat. Photon.* **11**, 752–762 (2017).
61. Özdemir, S. K., Rotter, S., Nori, F. & Yang, L. Parity-time symmetry and exceptional points in photonics. *Nat. Mater.* **18**, 783–798 (2019).
62. Miri, M.-A. & Alu, A. Exceptional points in optics and photonics. *Science* **363**, 363 (2019).
63. El-Ganainy, R., Khajavikhan, M., Christodoulides, D. N. & Özdemir, S. K. The dawn of non-Hermitian optics. *Commun. Phys.* **2**, 37 (2019).
64. Wiersig, J. Review of exceptional point-based sensors. *Photon. Res.* **8**, 1457–1467 (2020).
65. Gong, Z. et al. Topological phases of non-Hermitian systems. *Phys. Rev. X* **8**, 031079 (2018).
66. Ge, Z.-Y. et al. Topological band theory for non-Hermitian systems from the Dirac equation. *Phys. Rev. B* **100**, 054105 (2019).
67. Liu, T. et al. Second-order topological phases in non-Hermitian systems. *Phys. Rev. Lett.* **122**, 076801 (2019).
68. Liu, T., He, J. J., Yoshida, T., Xiang, Z.-L. & Nori, F. Non-Hermitian topological Mott insulators in one-dimensional fermionic superlattices. *Phys. Rev. B* **102**, 235151 (2020).
69. Tang, L.-Z., Zhang, L.-F., Zhang, G.-Q. & Zhang, D.-W. Topological Anderson insulators in two-dimensional non-Hermitian disordered systems. *Phys. Rev. A* **101**, 063612 (2020).
70. Tzortzakakis, A. F., Makris, K. G. & Economou, E. N. Non-Hermitian disorder in two-dimensional optical lattices. *Phys. Rev. B* **101**, 014202 (2020).
71. Tzortzakakis, A. F., Makris, K. G., Szameit, A. & Economou, E. N. Transport and spectral features in non-Hermitian open systems. *Phys. Rev. Research* **3**, 013208 (2021).
72. Luitz, D. J. & Piazza, F. Exceptional points and the topology of quantum many-body spectra. *Phys. Rev. Res.* **1**, 033051 (2019).
73. Daly, M. G., Jessop, P. E. & Yevick, D. Crosstalk reduction in intersecting rib waveguides. *J. Lightw. Technol.* **14**, 1695–1698 (1996).
74. Mingaleev, S. F., Schillinger, M., Hermann, D. & Busch, K. Tunable photonic crystal circuits: concepts and designs based on single-pore infiltration. *Opt. Lett.* **29**, 2858–2860 (2004).
75. Kobayashi, Y. & Tsuda, H. Crosstalk reduction using tapered intersecting waveguides. *Opt. Rev.* **12**, 387–390 (2005).
76. Longhi, S. Supersymmetric transparent optical intersections. *Opt. Lett.* **40**, 463–466 (2015).
77. Ren, J., Franke, S. & Hughes, S. Quasinormal mode theory of chiral power flow from linearly polarized dipole emitters coupled to index-modulated microring resonators close to an exceptional point. *ACS Photonics* **9**, 1315–1326 (2022).
78. Fernández-Alcázar, L. J., Kononchuk, R. & Kottos, T. Enhanced energy harvesting near exceptional points in systems with (pseudo-)PT-symmetry. *Commun. Phys.* **4**, 79 (2021).
79. Yoo, G., Sim, H. & Schomerus, H. Quantum noise and mode nonorthogonality in non-Hermitian PT-symmetric optical resonators. *Phys. Rev. A* **84**, 063833 (2011).
80. Schindler, J., Li, A., Zheng, M. C., Ellis, F. M. & Kottos, T. Experimental study of active lrc circuits with PT symmetries. *Phys. Rev. A* **84**, 040101 (2011).
81. Schindler, J. et al. PT-symmetric electronics. *J. Phys. A: Math. Theor.* **45**, 444029 (2012).
82. Chen, P.-Y. et al. Generalized parity-time symmetry condition for enhanced sensor telemetry. *Nat. Electron.* **1**, 297–304 (2018).
83. Xiao, Z., Li, H., Kottos, T. & Alù, A. Enhanced sensing and nondegraded thermal noise performance based on PT-symmetric electronic circuits with a sixth-order exceptional point. *Phys. Rev. Lett.* **123**, 213901 (2019).
84. Sakhdari, M. et al. Experimental observation of PT symmetry breaking near divergent exceptional points. *Phys. Rev. Lett.* **123**, 193901 (2019).
85. Pannatoni, R. F. Coupled mode theory for irregular acoustic waveguides with loss. *Acoust. Phys.* **57**, 36–50 (2011).

86. Fleury, R., Khanikaev, A. B. & Alù, A. Floquet topological insulators for sound. *Nat. Commun.* **7**, 11744 (2016).
87. Esmann, M., Lamberti, F. R., Lemaitre, A. & Lanzillotti-Kimura, N. D. Topological acoustics in coupled nanocavity arrays. *Phys. Rev. B* **98**, 161109 (2018).
88. Ma, G., Xiao, M. & Chan, C. T. Topological phases in acoustic and mechanical systems. *Nat. Rev. Phys.* **1**, 281–294 (2019).
89. Chen, Z.-G., Wang, L., Zhang, G. & Ma, G. Chiral symmetry breaking of tight-binding models in coupled acoustic-cavity systems. *Phys. Rev. Appl.* **14**, 024023 (2020).
90. Süsstrunk, R. & Huber, S. D. Classification of topological phonons in linear mechanical metamaterials. *Proc. Natl Acad. Sci. USA* **113**, E4767–E4775 (2016).
91. Schomerus, H. Nonreciprocal response theory of non-Hermitian mechanical metamaterials: response phase transition from the skin effect of zero modes. *Phys. Rev. Res.* **2**, 013058 (2020).
92. Gupta, A., Kurnosov, A., Kottos, T. & Thevamaran, R. Reconfigurable enhancement of actuation forces by engineered losses. Preprint at <https://arxiv.org/abs/2201.10744> (2022).
93. Wiersig, J., Kim, S. W., Hentschel, M. & Schomerus, H. Nonorthogonal pairs of copropagating optical modes in deformed microdisk cavities. *Phys. Rev. A* **78**, 053809 (2008).
94. Fan, S., Suh, W. & Joannopoulos, J. D. Temporal coupled-mode theory for the fano resonance in optical resonators. *JOSA A* **20**, 569–572 (2003).
95. Mailybaev, A. A. & Seyranian, A. P. *Multiparameter Stability Theory with Mechanical Applications* (World Scientific, 2004).
96. Shafarevich, I. R. & Remizov, A. O. *Linear Algebra and Geometry* (Springer, 2013).
97. Sunada, S. Enhanced response of non-Hermitian photonic systems near exceptional points. *Phys. Rev. A* **97**, 043804 (2018).
98. Heiss, W. D. Green's functions at exceptional points. *Int. J. Theoret. Phys.* **54**, 3954–3959 (2015).
99. Kato, T. *Perturbation Theory for Linear Operators* (Springer, 1995).
100. Baranov, D. G., Krasnok, A. & Alu, A. Coherent virtual absorption based on complex zero excitation for ideal light capturing. *Optica* **4**, 1457–1461 (2017).
101. Trainiti, G., Ra'di, Y., Ruzzene, M. & Alu, A. Coherent virtual absorption of elastodynamic waves. *Sci. Adv.* **5**, 1–7 (2019).
102. Zhong, Q., Simonson, L., Kottos, T. & El-Ganainy, R. Coherent virtual absorption of light in microring resonators. *Phys. Rev. Res.* **2**, 013362 (2020).
103. Metelmann, A. & Clerk, A. A. Quantum-limited amplification via reservoir engineering. *Phys. Rev. Lett.* **112**, 133904 (2014).
104. Soleymani, S. et al. Chiral and degenerate perfect absorption on exceptional surfaces. *Nat. Commun.* **13**, 1–8 (2022).
105. Li, B.-B. et al. Experimental observation of Fano resonance in a single whispering-gallery microresonator. *Appl. Phys. Lett.* **98**, 021116 (2011).
106. Peng, B., Özdemir, S. K., Chen, W., Nori, F. & Yang, L. What is and what is not electromagnetically induced transparency in whispering-gallery microcavities. *Nat. Commun.* **5**, 5082 (2014).
107. Wang, S., Zhao, T., Yu, S. & Ma, W. High-performance nano-sensing and slow-light applications based on tunable multiple Fano resonances and EIT-like effects in coupled plasmonic resonator system. *IEEE Access* **8**, 40599–40611 (2020).
108. Ma, K. et al. Tunable Fano and EIT-like resonances in a nested feedback ring resonator. *J. Lightw. Technol.* **40**, 2040–2044 (2022).
109. Kannan, B. et al. Waveguide quantum electrodynamics with superconducting artificial giant atoms. *Nature* **583**, 775–779 (2020).
110. El-Ganainy, R. & John, S. Resonant dipole-dipole interaction in confined and strong-coupling dielectric geometries. *New J. Phys.* **15**, 083033 (2013).
111. Hafezi, M., Demler, E., Lukin, M. & Taylor, J. Robust optical delay lines with topological protection. *Nat. Phys.* **7**, 1001–1005 (2011).
112. Zhao, H. et al. Non-Hermitian topological light steering. *Science* **365**, 1163–1166 (2019).
113. Jing, H. et al. Optomechanically-induced transparency in parity-time-symmetric microresonators. *Nat. Sci. Rep.* **5**, 1–7 (2015).
114. Jing, H., Özdemir, S. K., Lu, H. & Nori, F. High-order exceptional points in optomechanics. *Nat. Sci. Rep.* **7**, 1–10 (2017).
115. Schönleber, D., Eisfeld, A. & El-Ganainy, R. Optomechanical interactions in non-Hermitian photonic molecules. *New J. Phys.* **18**, 045014 (2016).
116. Minganti, F., Miranowicz, A., Chhajlany, R. & Nori, F. Quantum exceptional points of non-Hermitian Hamiltonians and Liouvillians: the effects of quantum jumps. *Phys. Rev. A* **100**, 062131 (2019).
117. Quiroz-Juárez, M. et al. Exceptional points of any order in a single, lossy waveguide beam splitter by photon-number-resolved detection. *Photon. Res.* **7**, 862–867 (2019).
118. Langbein, W. No exceptional precision of exceptional-point sensors. *Phys. Rev. A* **98**, 023805 (2018).
119. Lau, H.-K. & Clerk, A. A. Fundamental limits and non-reciprocal approaches in non-Hermitian quantum sensing. *Nat. Commun.* **9**, 4320 (2018).
120. Zhang, M. et al. Quantum noise theory of exceptional point amplifying sensors. *Phys. Rev. Lett.* **123**, 180501 (2019).
121. Wang, H., Lai, Y.-H., Yuan, Z., Suh, M.-G. & Vahala, K. Petermann-factor sensitivity limit near an exceptional point in a Brillouin ring laser gyroscope. *Nat. Commun.* **11**, 1610 (2020).
122. Wiersig, J. Robustness of exceptional-point-based sensors against parametric noise: the role of Hamiltonian and Liouvillian degeneracies. *Phys. Rev. A* **101**, 053846 (2020).
123. Smith, D. D., Chang, H., Mikhailov, E. & Shahriar, S. M. Beyond the Petermann limit: can exceptional points increase sensor precision? Preprint at <https://arxiv.org/abs/2005.12213> (2020).
124. Kononchuk, R., Cai, J., Ellis, F., Thevamaran, R. & Kottos, T. Enhanced signal-to-noise performance of EP-based electromechanical accelerometers. Preprint at <https://arxiv.org/abs/2201.13328> (2022).
125. Zhou, H., Lee, J. Y., Liu, S. & Zhen, B. Exceptional surfaces in PT-symmetric non-Hermitian photonic systems. *Optica* **6**, 190–193 (2019).
126. Zhang, X., Ding, K., Zhou, X., Xu, J. & Jin, D. Experimental observation of an exceptional surface in synthetic dimensions with magnon polaritons. *Phys. Rev. Lett.* **123**, 237202 (2019).
127. Qin, G.-Q. et al. Experimental realization of sensitivity enhancement and suppression with exceptional surfaces. *Laser Photon. Rev.* **15**, 2000569 (2021).

Acknowledgements

This work is supported by Air Force Office of Scientific Research (AFOSR) Multi-disciplinary University Research Initiative (MURI) Award on Programmable systems with non-Hermitian quantum dynamics (Award No. FA9550-21-1-0202). R.E. also acknowledges support from ARO (Grant No. W911NF-17-1-0481), NSF (Grant No. ECCS 1807552), and the Alexander von Humboldt Foundation. S.K.O. acknowledges support from NSF (Grant No. ECCS 1807485) K.B. acknowledges support by the Leibniz Association within the SAW-project LAPTON and from the Alexander von Humboldt Foundation.

Author contributions

R.E. conceived the project. R.E. and A.H. performed the theoretical analysis with feedback from S.K.O., K.B., and D.N.C. The numerical simulations were performed by A.H. All authors contributed to the manuscript writing.

Competing interests

The authors declare no competing interests.

Additional information

Supplementary information The online version contains supplementary material available at <https://doi.org/10.1038/s41467-022-30715-8>.

Correspondence and requests for materials should be addressed to A. Hashemi or R. El-Ganainy.

Peer review information *Nature Communications* thanks Wenjie Wan, Tsampikos Kottos, Ronny Thomale and the other anonymous reviewer(s) for their contribution to the peer review of this work.

Reprints and permission information is available at <http://www.nature.com/reprints>

Publisher's note Springer Nature remains neutral with regard to jurisdictional claims in published maps and institutional affiliations.



Open Access This article is licensed under a Creative Commons Attribution 4.0 International License, which permits use, sharing, adaptation, distribution and reproduction in any medium or format, as long as you give appropriate credit to the original author(s) and the source, provide a link to the Creative Commons license, and indicate if changes were made. The images or other third party material in this article are included in the article's Creative Commons license, unless indicated otherwise in a credit line to the material. If material is not included in the article's Creative Commons license and your intended use is not permitted by statutory regulation or exceeds the permitted use, you will need to obtain permission directly from the copyright holder. To view a copy of this license, visit <http://creativecommons.org/licenses/by/4.0/>.

© The Author(s) 2022